Marine Geology 412 (2019) 95–106

Contents lists available at ScienceDirect

Marine Geology

journal homepage: www.elsevier.com/locate/margo

Coupling between tidal mudflats and salt marshes affects marsh morphology

Mark Schuerch[a,b,*], Tom Spencer[b], Ben Evans[b]

[a] Lincoln Centre for Water and Planetary Health, School of Geography, University of Lincoln, Brayford Pool Campus, Lincoln, United Kingdom
[b] Cambridge Coastal Research Unit, Department of Geography, University of Cambridge, Downing Place, Cambridge, United Kingdom

ARTICLE INFO

Editor: Shu Gao

Keywords:
Salt marsh
Tidal mudflat
Sediment deposition
Intertidal sediment resuspension
Lateral marsh erosion
Wave activity

ABSTRACT

It is generally assumed that coastal salt marshes are capable of adapting to moderately fast rising sea levels although local sediment availability crucially affects this capability. While there is an increasing awareness that local sediment availability is inherently related to sediment dynamics on the adjacent tidal mudflat, our current understanding of the interactions between salt marshes and tidal flats is very limited. To address this knowledge gap, we measured suspended sediment concentrations alongside hydrodynamic, morphological and sediment deposition measurements over a total period of 16 weeks in a wave-exposed macro-tidal mudflat-salt marsh system on the UK east coast (Tillingham).

Our results show that local sediment supply to the salt marsh is strongly linked to intertidal sediment dynamics and that the vast majority of suspended sediment deposited on the marsh originates from wind-wave induced intertidal sediment resuspension in very close vicinity (< 130 m) to the seaward marsh margin. Vertically the salt marsh grows at rates > 5 mm yr^{-1}, thereby increasing the slope of the tidal mudflat-salt marsh transition and making the salt marsh susceptible to lateral erosion. Consequently, the marsh edge retreats at a rate of approximately 0.8 m yr^{-1}. Our study shows that the response of coastal salt marshes to climate change is a function of the coupled tidal mudflat-salt marsh system, rather than their vertical sediment accretion rates alone. Therefore, the idea that salt marsh adaptability relies on local sediment supply needs to be expanded, incorporating the morphology and long-term evolution of the adjacent tidal mudflats.

1. Introduction

Coastal salt marshes are increasingly considered as valuable ecosystems at the interface between land and sea; they are known to sequester atmospheric carbon, contribute to global biodiversity, improve coastal water quality, and provide protection against coastal flooding and erosion (Barbier et al., 2011). Under ongoing global sea level rise (SLR; Church et al., 2013) concerns have been expressed, first voiced by Stevenson et al. (1986), that coastal salt marshes may experience 'accretionary deficit' (i.e. not being able to sufficiently adapt their elevation through vertical sediment accretion), become inundated permanently and convert to open water (Crosby et al., 2016; Spencer et al., 2016; Schepers et al., 2017). However, the increase in surface elevation, particularly of minerogenic coastal salt marshes (i.e. salt marshes 'dominated by tidally introduced mineral matter' (Allen, 2000)), is driven by the deposition of suspended sediment during inundation events. This process may accelerate under increased rates of SLR and associated higher inundation frequencies (Kolker et al., 2010; Hill and Anisfeld, 2015). The environmental variables primarily controlling the ability of minerogenic coastal salt marshes to vertically adapt to SLR are commonly assumed to be local tidal range, sediment availability and inundation frequency (French, 1993; French, 2006; Kirwan et al., 2010; D'Alpaos et al., 2011; Schuerch et al., 2013; Schuerch et al., 2018).

It has been variously hypothesised that increased local tidal range will (i) increase sediment resuspension through higher tidal current velocities, hence improving sediment availability (Friedrichs and Perry, 2001; Temmerman et al., 2003a, 2003b; Schuerch et al., 2013); (ii) reduce SLR-induced channel erosion, due to a proportionally smaller increase of the tidal prism (Kirwan and Guntenspergen, 2010); and (iii) increase the elevation range where salt marsh vegetation can grow (Friedrichs and Perry, 2001; Kirwan and Guntenspergen, 2010). Greater sediment availability, seen in higher suspended sediment concentrations (SSCs), will increase the amount of mineral sediment being deposited on the marsh surface during a single inundation (French, 1993; French, 2006; Kirwan and Murray, 2007), assuming an invariant sediment trapping efficiency (i.e. 'percentage of the sediment introduced on flood tide retained on the marsh surface' (French, 2006: p. 127)). Finally, it can be argued that if the marsh is inundated more regularly,

* Corresponding author at: Lincoln Centre for Water and Planetary Health, School of Geography, University of Lincoln, Brayford Pool Campus, Lincoln, United Kingdom.
E-mail address: mschuerch@lincoln.ac.uk (M. Schuerch).

https://doi.org/10.1016/j.margeo.2019.03.008
Received 30 May 2018; Received in revised form 6 November 2018; Accepted 17 March 2019
Available online 23 March 2019

sediment deposition events will become more frequent and thus the rate of sedimentation will increase.

Supply of suspended sediment for coastal salt marshes is highly variable in space and time, owing to the multitude of processes involved in coastal sediment transport and sediment resuspension (Wang et al., 2012), as well as the large variability associated with meteorological and climate drivers (Schuerch et al., 2016; Zhou et al., 2016; Ma et al., 2018). Despite knowledge about the crucial importance of sediment supply and its pronounced temporal variability for minerogenic marshes, most model-based assessments on the ability of coastal wetlands to adapt to future SLR assume a constant sediment supply (French, 1993; French, 2006; Mariotti and Fagherazzi, 2010; D'Alpaos et al., 2011; Mariotti and Carr, 2014; Rodríguez et al., 2017). Where temporal variations in sediment supply are accounted for, sediment supply is assumed to be driven by current-induced intertidal sediment resuspension (Temmerman et al., 2003a, 2003b; D'Alpaos et al., 2007; Schuerch et al., 2013). However, other studies have suggested that wave-induced sediment resuspension may be more important for marsh sediment supply (Callaghan et al., 2010; Ma et al., 2018) but field data on how wave-induced sediment resuspension affects the morphological development of salt marshes are rare. Furthermore, in order to improve our understanding of the impacts that temporal variations in sediment supply may have on the ability of coastal salt marshes to adapt to future SLR, exact knowledge on the sources of the supplied sediment is necessary, including the relative contributions from both wave- and current-induced sediment resuspension (Schuerch et al., 2014).

It has previously been argued that the sources of mineral suspended sediment supplied to a salt marsh can broadly be divided into external ('far field') and proximate ('near field') sediment sources (Schuerch et al., 2014). External sediment sources include contributions from riverine sediment discharge (Bergamino et al., 2017), coastal erosion along neighbouring coastlines, offshore sediment sources and atmospheric deposition (Pedersen and Bartholdy, 2006; Schuerch et al., 2014; Schuerch et al., 2016). Proximate sediment sources include sediment resuspension on tidal mudflats and erosion of marsh cliffs and tidal creeks (Friedrichs and Perry, 2001; Pedersen and Bartholdy, 2006; Mariotti and Carr, 2014; Schuerch et al., 2014).

The aim of this study was to identify the role of intertidal sediment resuspension in contributing sediment to a salt marsh on the UK east coast from an adjacent, proximate mudflat. Further, we aimed to identify the drivers of temporal variations in intertidal sediment resuspension, particularly focusing on changes in hydrodynamic and meteorological conditions, and to assess how these variations influence sediment deposition processes on the marsh platform. More specifically, the research questions to be answered included: (i) what are the drivers for the temporal variability in sediment supply?; (ii) how does this observed temporal variability affect sediment deposition patterns on the salt marsh platform?; and (iii) what are the implications of the observed temporal variability for the long-term morphological development of the salt marsh?

2. Regional setting

The study site was a macro-tidal salt marsh on the UK east coast between the Blackwater and the Crouch estuaries (Dengie Peninsula) on the northern margin of the Greater Thames Estuary, near the village of Tillingham (Fig. 1). The mean spring tidal range there is 4.8 m, and the neap tidal range 2.9 m (Towler and Fishwick, 2017). This open coast marsh is exposed to a moderate wave climate with a mean significant wave height of 0.18 m and a maximum significant wave height of 0.73 m (October 2012–July 2016), as measured at the marsh edge (unpublished data).

The salt marsh is located to seaward of an earthen embankment (seawall) and has varying widths of up to 700 m. Adjacent to the vegetated marsh platform, an extensive tidal mudflat extends into the North Sea for up to 3.7 km offshore (Möller, 2006). The transition zone from tidal mudflat to vegetated salt marsh is characterized by a shore-normal system of ridges and runnels (Fig. 2). The elevations of the marsh platform range from 1.9 m in the pioneer vegetation zone to 2.5 m above Ordnance Datum Newlyn (ODN; where 0.0 ODN approximates mean sea level) in the mid and high marsh vegetation zones (Fig. 2).

3. Materials and methods

3.1. Experimental setup

Field measurements of the hydrodynamics and the morphological development of the tidal mudflat; SSCs along a 177 m long, shore-normal transect; and sediment deposition on the marsh platform were conducted over a 5-week period in summer (25/05–28/06/2016) and an 11-week period in autumn/winter (20/09–06/12/2016). The most seaward-located measuring station was 130 m from the edge of the vegetated marsh platform (marsh edge) on the tidal mudflat (ASM2113). The most landward location was situated in the mid marsh vegetation zone (a mixed canopy dominated by *Puccinellia maritima*), 47 m inland from the marsh edge and 210 m seaward of the seawall (SET2; Fig. 2).

3.2. Hydrodynamic measurements

Water levels along the entire transect were measured using four pressure sensors (Solnist Levellogger, Model 3001), programmed to record water levels every 30 s (Fig. 2). The measured raw data from the pressure sensors were corrected for variations in atmospheric pressure and smoothed with a 15-min moving average filter to derive still water levels, maximum inundation depths of tidal inundations (HW levels), tidal asymmetry (i.e. ebb duration/flood duration) and the frequency of inundation of the marsh surface at the marsh edge (ASM2115). Based on the unsmoothed water levels, and using the method of Reef et al. (2018), the temporal variability in wave activity during the experiment was approximated with a wave proxy, calculated as the tide-averaged absolute water level deviations from the still water level.

The data collected at a recording frequency of 4 Hz by the bottom-mounted PDCR 1830 pressure transmitter (GE Druck) during the high-water stages of selected tidal inundations (Fig. 2) were processed to produce summary wave parameters, following the methodology of Möller et al. (1999). From these wave parameters, the root mean square wave height (H_{rms}) was used to calibrate the wave proxy. The calibration showed that the wave proxy (WP), calculated at ASM2113, was linearly correlated with H_{rms}, recorded by the PDCR 1830. The linear regression showed that $H_{rms} = 6.645 * WP$ ($R^2 = 0.93$), as reported by Reef et al. (2018).

Tidal currents were measured on the tidal mudflat at ASM2113, using an Acoustic Doppler Current Profiler (ADCP), namely an Aquadopp Profiler 2 MHz (Nortek AS), with a recording interval of 30 s. Various measurement settings were tested to optimize the measurement accuracy and precision, including cell size and measurement load (ping rate). The resulting measurement precision typically ranged between 1 and 2 cm s^{-1} with a nominal accuracy of 0.5 cm s^{-1} (Nortek technical specification).

3.3. Turbidity measurements

Turbidity measurements were conducted using two turbidity profilers, namely two Argus Suspension Meters (ASM) IV (ARGUS Gesellschaft für Umweltmeßtechnik mbH). The profilers consist of 144 optical backscatter sensors, arranged as a vertical array with a spacing of 1 cm. One turbidity profiler (ASM2113) was deployed on the mudflat (130 m from the marsh edge); the other (ASM2115) was located in the transition zone between the annual pioneer vegetation and the perennial marsh vegetation, the boundary defined as the marsh edge for

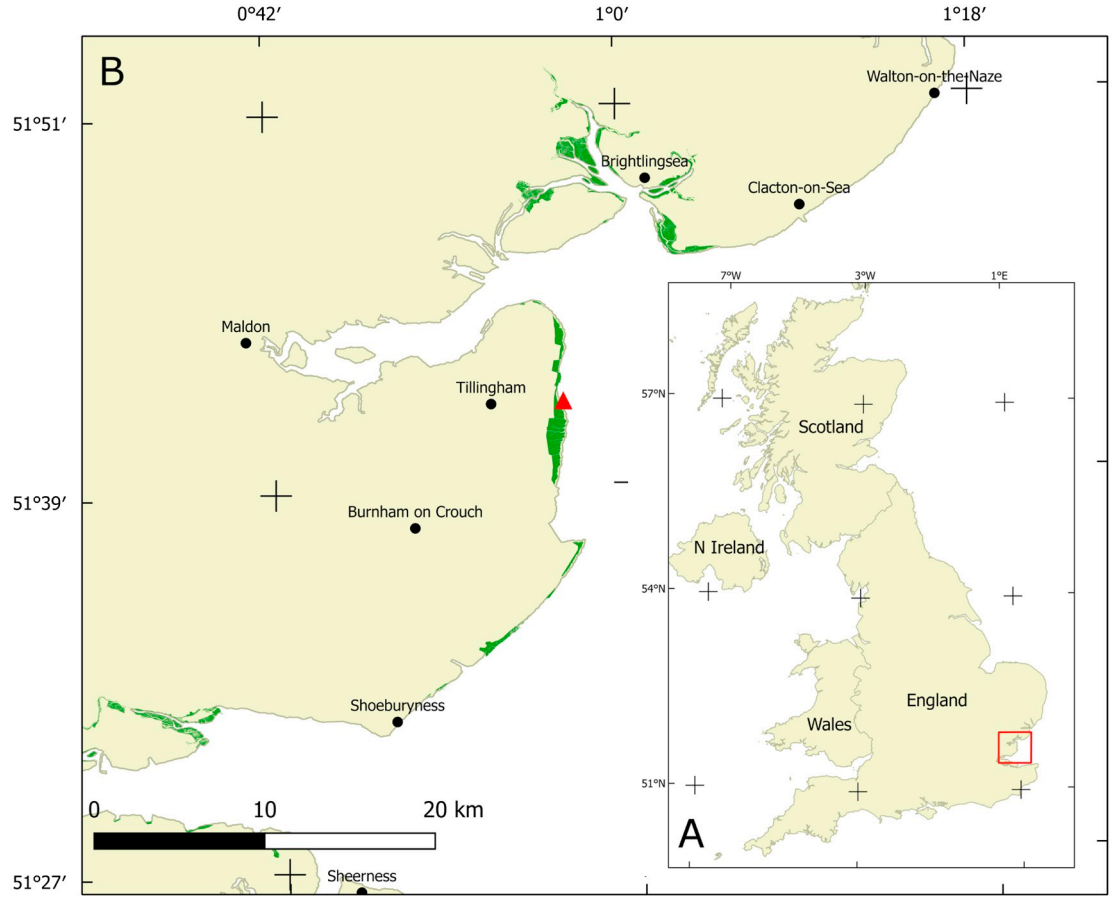

Fig. 1. Study area. (A) Location of the study site in southeast England, on the northern margin of the Greater Thames Estuary and (B) distribution of coastal salt marshes (green areas) on the Essex coast, including the location of the study site (red triangle) on the salt marsh near Tillingham. (For interpretation of the references to colour in this figure legend, the reader is referred to the web version of this article.)

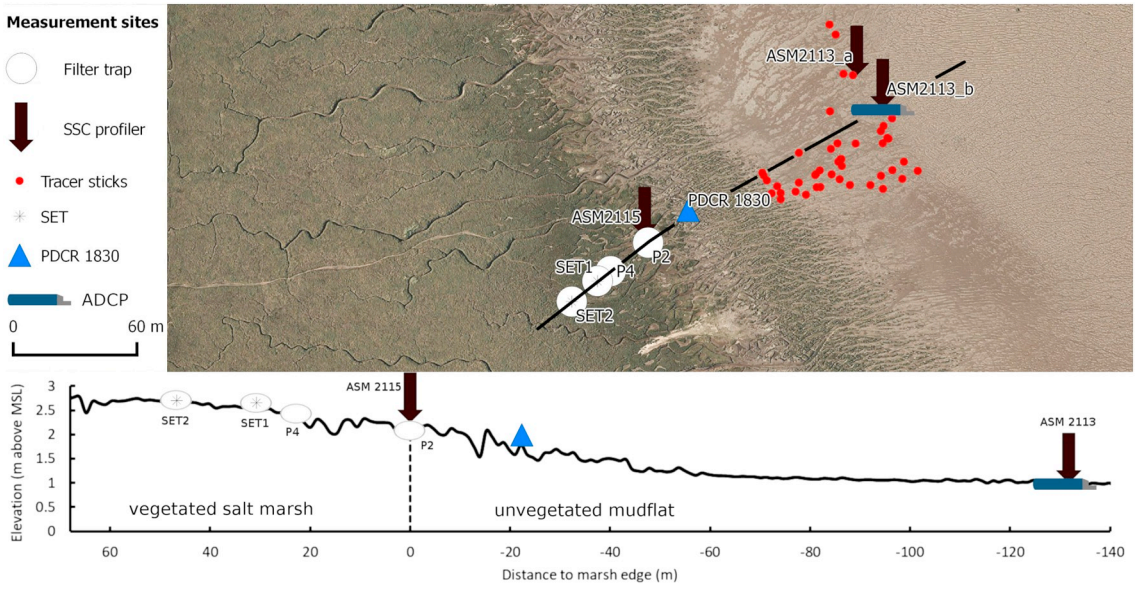

Fig. 2. Experimental design. Aerial photograph from 2016 (Environment Agency, 2016a) of the studied salt marsh, the locations of the measurement devices and the topographical profile of the tidal mudflat, the transition to the salt marsh and the seaward part of the vegetated marsh platform, based on a 1 m digital terrain model (Environment Agency, 2016b). The seaward turbidity profiler (ASM2113) and ADCP (Nortek Aquadopp Profiler) were moved from position ASM2113_a to ASM2113_b on 03/06/2016. One Solnist pressure sensor was placed at each of the sites ASM2113, ASM2115/P2, P4 and SET2. The pressure transducer PDCR 1830 was located in the transition zone from the tidal mudflat to the vegetated salt marsh.

the purpose of this experiment (Fig. 2). Data were recorded every 30 s, averaging 10 measurements at 1 Hz within 10 s. All measurements were discarded when inundation depths were lower than 3 cm.

Conversion of the turbidity data (ftu) to SSC ($mg\,l^{-1}$) was performed based on 53 1-litre water samples, collected with an automated water sampler (Teledyne ISCO, model 6712) during three time periods in April (7–11), July (21–24) and December (12–17) 2016. Water samples were filtered using pre-weighed GF/C filters, dried at 105 °C for 24 h and subsequently re-weighed. For the 5-week measurement period in summer, the SSCs derived from 34 water samples from April and July were used for the instrument calibration (Reef et al., 2018); for the autumn and winter measurement period, the SSCs derived from 19 water samples from December were utilized (unpublished data).

3.4. Measurements of sediment deposition on the salt marsh surface and elevation change

Sediment deposition was measured using filter traps, deployed on the marsh surface at three different locations along a cross-shore transect, starting from the landward turbidity profiler (ASM2115) and proceeding in a landward direction (Fig. 2). During the summer period, measurements were conducted at the sites ASM2115, P4 and SET1, whereas during the autumn/winter period, the site SET1 was exchanged for SET2 (Fig. 2). At each location, three filter traps were installed to capture the small-scale spatial variability in deposition and to derive an average local deposition. The filter traps consisted of pre-weighed glass-fibre filters (Whatman GF/F) with a diameter of 9 cm, being placed on an equally sized petri dish and fixed with three metal pegs (Nolte et al., 2013). Following their deployment, the filter traps were usually retrieved after five days, although retrievals varied between two and ten days.

Alongside the transect of filter traps, a Rod Surface Elevation Table (RSET; Cahoon et al., 2002), was used in combination with feldspar marker horizons (MH) at two different sites (SET1 and SET2, Fig. 2) to monitor surface elevation changes and sediment accretion rates between December 2015 and February 2017, with measurements on 18 December 2015, 11 July 2016 and 17 February 2017. In contrast to the filter traps, the coupled RSET and MH method reveals the longer-term salt marsh surface elevation change and near-surface vertical accretion rate respectively (Cahoon et al., 1995). Average surface elevations and standard deviations were calculated from 36 measurements for each RSET site, consisting of nine measurements at four locations around the site. Similarly, average accretion rates and standard deviations were calculated from 12 MH measurements per site, namely three replicates at four locations around the site (same locations as used for the RSET measurements).

3.5. Measurement of mudflat surface elevation

The sediment dynamics on the tidal mudflat were monitored using coloured sand tracer sticks that were vertically inserted into the mudflat, until the upper end of the column was level with the mudflat surface. Sampling was conducted at four locations between ASM2113 and the marsh edge, with three replicates at each location (Fig. 2). The tracer sticks (88 mm in length, 10–20 mm in width, 5–10 mm in thickness) consisted of a mixture of coloured sand and a highly concentrated sugar solution, which were “baked” in a plastic tray for three days at 50 °C. Upon insertion into the mudflat, the solidified sand tracers, cemented by the sugar solution, dissolved as the sugar solution dissolved in the water-saturated sediment, and the coloured sand was left as an indicator for sediment mobilization and deposition (Runte, 1989; Schwarzer et al., 2003). In contrast to the tidal mudflat under investigation, the tracer sticks consisted of non-cohesive sand particles to ensure rapid dissolution of the binding material (the sugar solution). Meanwhile, the effect of the potentially higher erodibility of the tracer stick material was counteracted by the small width and thickness of the tracer sticks.

After five days (occasionally two or ten days), a 20 cm long sediment core was extracted at each tracer location, using a PVC tube with an inner diameter of 7.0 cm, to retrieve the remaining tracer stick. In the laboratory, each core was opened through its centre to measure the remaining length of the tracer stick (L) as well as the thickness, if any, of the sediment layer deposited above the tracer (T). The net erosion (E = negative) or deposition (E = positive) was calculated based on the initial length of the tracer stick (IL): $E = IL - (L + T)$.

3.6. Meteorological data

Meteorological data (recorded wind speeds and wind directions) for the time period of the experiment were obtained from the weather station at Shoeburyness, Thames Estuary (Met Office, 2006), 17 km SE of the study site (Fig. 1). It was assumed that the study site was exposed to the same wind condition as at Shoeburyness.

3.7. Long-term marsh edge dynamics

The overall change in marsh edge position was determined for the time period 1992 to 2013 over the 11 km long eastward facing edge of the Dengie Peninsula that is fronted by marsh. The seaward limit of macrophytic vegetation was manually digitised from UK Environment Agency vertical aerial photography for both years (25 cm resolution panchromatic in 1992 and 20 cm RGB in 2013, late summer acquisitions). The Digital Shoreline Analysis System (DSAS; Thieler et al., 2009) was then used to cast shore-normal transects at 10 m alongshore spacing and calculate the rate of change (Net Shoreline Movement (NSM; m)) at each transect intersection with the digitised shorelines. Transects where shoreline change resulted in a transect crossing a creek between intersections with the two shorelines were discarded. A total of 1058 transects were retained for analysis.

3.8. Statistical methods

The hydrodynamic forcing and the turbidity data (water level, wave activity and SSC) were aggregated for each tidal inundation as well as for each sampling period of the measurements on marsh and mudflat morphodynamics (Table 1). This enabled us to directly relate the hydrodynamic forcing to the data collected on the morphological responses of the salt marsh and the mudflat, for time periods of between 2 and 10, but usually 5, days.

The statistical analyses of the collected data included:

(i) Identification of drivers for intertidal sediment resuspension: (non-) linear regression analysis between the median SSC (per tide) at ASM2113 and the hydrodynamic forcing (Table 1).
(ii) Comparison between landward and seaward turbidity sensors: linear regression analysis between median SSC (per tide) at ASM2113 and ASM2115.
(iii) Identification of drivers for the observed differences: stepwise linear regression analysis with SSC difference (per tide) as the dependent variable and all variables for hydrodynamic forcing (Table 1) as independent variables.
(iv) Analysis of drivers for temporal variability of average sediment deposition on the salt marsh (per sampling period): stepwise linear regression analysis with average sediment deposition as dependent variable and SSC variables (Table 1) plus inundation frequency (IF) at ASM2115 as independent variables.
(v) Trend analysis of the spatial patterns of sediment deposition, averaged over the entire experiment using boxplots and the non-parametric Kruskal-Wallis test.
(vi) Identification of significant trends for sediment deposition as a function of distance from the marsh edge: (a) linear regression analysis to test for a significant ($p < 0.05$) linear (positive or

Table 1
Aggregation of high frequency raw data on hydrodynamic forcing and turbidity as well as the morphological data on marsh and mudflat dynamics.

Var. group	Variable	Level of aggregation		Sampling period (2–10 days, usually 5 days)
		Raw data	Single tidal inundation	
Hydrodynamic forcing	Still water level (ASM2113)	Moving-average filter with 15-min window size applied to raw water level data	- Maximum inundation depth (**HW level**) - Tidal asymmetry (ebb/flood duration)	- Mean height of HW levels (**avg. HW level**) - Highest HW level (max. **HW level**) - Inundation frequency (**IF**)
	Wave proxy (ASM2113)	Raw water level data (1/30 Hz)	Mean deviation of raw water level data from still water level (**Wave proxy**)	- Mean wave proxy (**avg. WP**) - Maximum wave proxy (**max. WP**)
	Depth-normalized wave proxy (ASM2113)		Wave proxy divided by HW level (**norm. Wave proxy**)	- Mean normalized wave proxy (**avg. norm. WP**)
Turbidity	Suspended sediment concentrations (SSC)	Depth-averaged SSC (1/30 Hz) derived from SSC profiles	Median depth-averaged SSC (**median SSC**)	- Mean of median SSC (**avg. SSC**) - Maximum of median SSC (**max. SSC**)
	Landward SSC increase		Difference in median SSC between the seaward and the landward turbidity profilers (**SSC difference**)	- Mean SSC difference (**avg. SSC difference**) - Maximum SSC difference (**max. SSC difference**)
Marsh and mudflat morphology	Sediment deposition on salt marsh	Filter trap data for sampling periods between 2 and 10 days		- Mean sediment deposition for each site and period, including data of all three traps per site (**sediment deposition**) - Mean sediment deposition of all traps for one period (**avg. sediment deposition**)
	Mudflat morphology	Tracer stick data for sampling periods between 2 and 10 days		- Thickness of sediment on top of the eroded tracer stick (**top layer**) - Change in mudflat surface elevation (**erosion** = initial stick length – (remaining stick length + top layer))

negative) trend; (b) nonlinear regression analysis for all insignificant periods testing for a significant (convex or concave) 2nd order polynomial relationship.

(vii) Analysis of drivers for spatial sediment deposition patterns (as identified in (vi)): non-parametric Kruskal-Wallis test applied to all variables for hydrodynamic forcing and turbidity (Table 1), categorized based on the identified spatial sediment deposition patterns.

Following every stepwise linear regression analysis, all variables included in the resulting regression models were tested for correlation (Pearson correlation coefficient). Where model variables were significantly correlated ($p < 0.05$), the variable with the higher p-value was removed from the model and the stepwise linear regression was repeated until all model variables were independent from each other.

4. Results

4.1. Hydrodynamic forcing

The entire measurement period included seven complete spring-neap tidal cycles. These were characterized by higher neap high water (HW) levels and lower spring HW levels during the summer period and lower neap HW levels combined with higher spring HW levels during the autumn and winter. While the seaward turbidity profiler (ASM2113) was inundated on every tide, the landward profiler (ASM2115) was only inundated during tides exceeding 1.2 m inundation depth at ASM2113. The average inundation depth at ASM2113 was 1.28 m, with a maximum of 2.13 m during the first tidal inundation on 17/11/2016 and a minimum of 0.38 m during the first tide on 11/10/2016. Tidal flow velocities on the mudflat (at ASM2113) were very low and could not be determined using the instrument's precision of 1–2 cm s^{-1} and its accuracy of 0.5 cm s^{-1}.

Although, the wave activity measured at ASM2113 was not correlated with the measured HW levels (Pearson's $r = -0.1043$, $p = 0.14$), the maximum wave activity appeared to be related to inundation depth, with higher waves possible when inundation depths were large. The upper boundary values of the measured wave proxy (WP_{max}) thereby followed a linear relationship with inundation depth (h): $WP_{max} = 0.045 * h$.

Wave activity in summer was not significantly different (Kruskal-Wallis: $p = 0.79$) from wave activity in autumn/winter ($WP = 0.022$ in summer, compared to 0.023 in winter). The maximum wave activity in summer ($WP = 0.058$) was recorded during the first tide on 02/06/2016, whereas the maximum wave activity in autumn/winter ($WP = 0.064$) occurred during the first tide on 20/11/2016. Sustained periods (> 2 days) of increased wave activity ($WP > 0.025$), identified using a smoothed WP time series (moving average: window size of 10 tides), were 24/05–05/06/2016, 03/10–08/10/2016, 11/10–16/10/2016 and 18/11–28/11/2016.

The measured wave proxy was significantly correlated with the recorded wind speed (v, knots) and wind direction (Θ in degrees azimuth) at Shoeburyness. Higher wind speeds created higher waves when blowing onshore and lower waves when blowing offshore:

$$WP = m * [v * (\sin((\Theta * 180)/\pi) + 1.4)] + a \quad (1)$$

where $m = 0.000879$ is the slope and $a = 0.0125$ the intersect of the linear regression between the sinus-transformed wind speed (term within square brackets) and the wave proxy ($R^2 = 0.54$, $p < 0.001$).

4.2. Suspended sediment concentrations

On the tidal mudflat (ASM2113) the median depth-averaged SSC ranged from 0.03 to 279 mg l^{-1} in summer and from 2.6 to 1039 mg l^{-1} in autumn/winter. In both seasons SSC showed a strong positive relationship with wave activity. In autumn/winter, strong wave activity

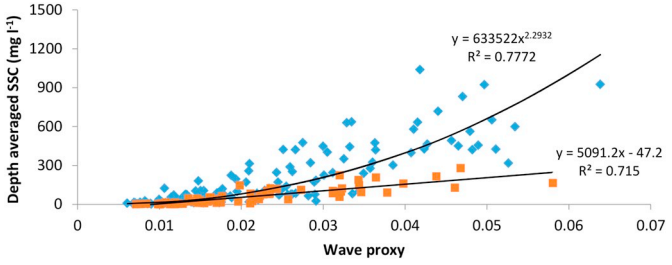

Fig. 3. Intertidal sediment resuspension. Relationship between wave proxy and median depth-averaged SSC. Each data point represents one tidal inundation. Data are separated between summer (orange squares) and autumn/winter (blue diamonds) measurements. (For interpretation of the references to colour in this figure legend, the reader is referred to the web version of this article.)

had a greater impact on SSC than in summer (Fig. 3). The relationship between the wave proxy and the median depth-averaged SSC followed a linear trend in summer ($R^2 = 0.72$) and a power function in winter ($R^2 = 0.77$) as a best fit (Fig. 3).

The highest SSC at ASM2113 (1039 mg l^{-1}) was recorded for the first tide on 22/11/2016 during a period of three days (20/11–22/11/2016) when the median SSC was > 900 mg l^{-1} for every tidal inundation. During the same time period, the highest SSC was also recorded at the landward turbidity profiler, located at the marsh edge (ASM2115). At this location the maximum SSC was 1445 mg l^{-1}. Generally, the SSC records at ASM2113 (mudflat) and ASM2115 (marsh edge) were significantly correlated with each other ($R^2 = 0.83$, $p < 0.001$). However, on average, SSC at the marsh edge was 25% higher than on the mudflat (Fig. 4), indicating a general landward increase in SSC. The general trend towards a landward increase in SSC was also represented in the median concentrations of 42 and 74 mg l^{-1} for the sensors on the mudflat and at the marsh edge respectively.

The greatest difference between the landward and the seaward sensors (i.e. landward increase in SSC) was observed during the first tide on 20/11/2016, when SSC at the landward sensor was 519 mg l^{-1} higher than on the mudflat. Meanwhile, the largest difference for the summer period was recorded for the first tide on 31/05/2016. When comparing the differences in SSC between the landward (ASM2115) and the seaward (ASM2113) sensors with the hydrodynamic forcing (i.e. HW level, wave proxy, depth-normalized wave proxy at ASM2113), the depth-normalized wave proxy (WP_{norm}) best explained the observed variations ($R^2 = 0.22$, $p < 0.0001$). Moreover, the upper boundary of the landward sediment transport (y_{max}) was defined by WP_{norm} ($y_{max} = 16{,}000 * WP_{norm}$).

4.3. Sediment deposition

4.3.1. Temporal sediment deposition pattern

The average sediment deposition (g) on all filter traps during the measurement period ranged between 0.03 and 1.32 g, averaging 0.41 g per sampling period. The highest sediment deposition took place between 24/05 and 3/06/2016 (1.11 g) in summer and between 15/11 and 21/11/2016 (1.32 g) in autumn/winter. Interestingly, the sediment deposition in summer was not significantly (Kruskal-Wallis: $p = 0.93$) different from that in autumn/winter, although the median and the maximum deposition were higher (Fig. 5).

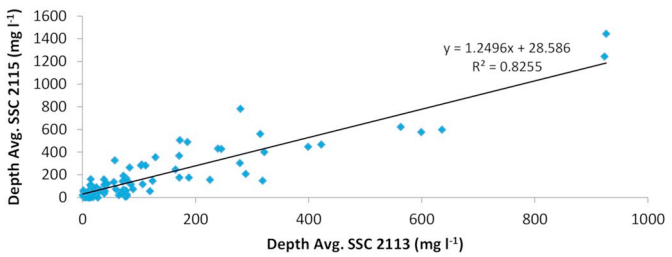

Fig. 4. Landward SSC increase. Linear relationship between depth-averaged SSC at ASM2113 (mudflat) and ASM2115 (marsh edge) for the entire measurement period (summer and autumn/winter).

The average sediment deposition was significantly correlated with the maximum SSC at the landward sensor (ASM2115), and the number of inundations during each sampling period (inundation frequency). The linear regression model including these two parameters explained 69% of the observed variability in sediment deposition (Fig. 5). While representing the more important driver for sediment deposition on the marsh, the maximum SSC at ASM2115 (C_{max}) was linearly related to the maximum increase in SSC between the seaward and the landward turbidity sensors (max. landward SSC increase: C_{diff}): $C_{max} = 2.02 * C_{diff} + 77.9$ ($R^2 = 0.66$, $p < 0.001$).

4.3.2. Spatial sediment deposition pattern

Averaged over the entire measurement period, the sediment deposition recorded on the filter traps at the different locations within the marsh did not significantly differ between each other (Kruskal-Wallis: $p = 0.23$), suggesting no systematic differences between the different sites, and most importantly, no landward decrease in sediment deposition (Fig. 6).

The trends for sediment deposition as a function of distance from the marsh edge for every sampling period individually are shown in Fig. 7. A significant linear decrease from the marsh edge inland was only observed between 21/11 and 26/11/2016, whereas a linear increase was observed for two sampling periods (03/06–08/06/2016 and 10/11–15/11/2016). During four sampling periods, we found a polynomial rather than a linear sedimentation pattern. The maximum sediment deposition was measured in the centre of the marsh (concave polynomial pattern) during the two sampling periods 20/09–24/09/2016 and 24/09–04/10/2016, whereas the minimum sediment deposition was in the centre of the marsh (concave polynomial pattern) during the sampling periods 09/10–19/10/2016 and 15/11–21/11/2016. However, for most sampling periods we could not determine any significant linear or polynomial trends (Fig. 7); and the observed spatial deposition patterns were not significantly related to any hydrodynamic forcing or turbidity variable (Table 1).

4.4. Mudflat morphology

On the mudflat, adjacent to the salt marsh, net erosion was the dominant process observed during the measurement period (Fig. 8), although the difference between summer and winter erosion was insignificant (Kruskal-Wallis: $p = 0.23$). However, the strongest erosion events were recorded in autumn/winter, namely between 21/11 and 26/11/2016 (1.5 cm, on average) and between 4/10 and 9/10/2016 (1.0 cm, on average). These periods coincided with the two periods showing the highest average wave proxy during the entire measurement period (Fig. 8). Meanwhile, net sediment deposition was observed during two periods only, namely between 14/10 and 21/10/2016 (1 cm, on average) and between 10/11 and 15/11/2016 (0.6 cm, on average). Both of these periods were characterized by relatively high maximum tidal HW levels, i.e. two of the four highest inundation periods show net deposition (Fig. 8). However, none of the data series for HW levels (average and maximum HW levels), wave activity (average and maximum wave proxy) and sediment resuspension (average and maximum SSC at ASM2113) were significantly correlated with the measured mudflat erosion (Fig. 8).

4.5. Surface elevation change and vertical accretion

Surface elevation change over the period of our experiment was 5.6 ± 1.5 (1 (standard deviation) mm yr^{-1} at SET1 and ca. 5.3 ± 2.3 mm yr^{-1} at SET2 (Table 2: RSET rates). Meanwhile, the

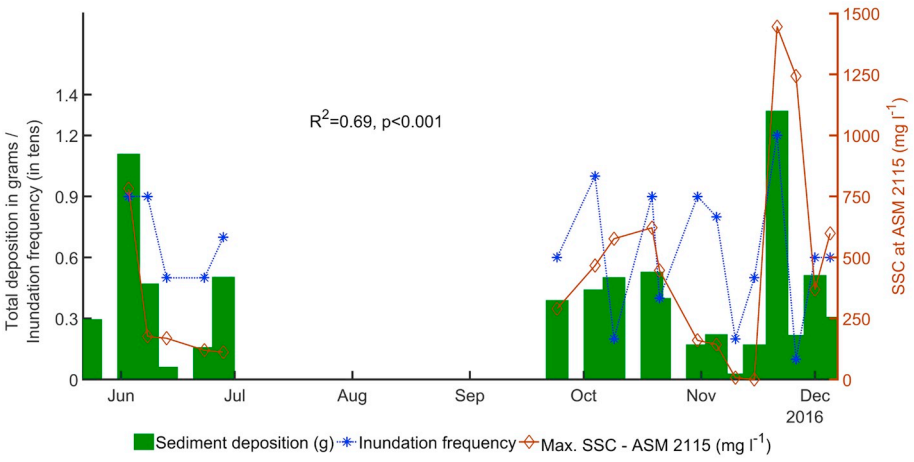

Fig. 5. Sediment deposition on the salt marsh. Average sediment deposition (g) of all filter traps on the vegetated salt marsh (D: green bars), the maximum SSC (C_{max}: brown line, in mg l^{-1}) and the inundation frequency (IF: blue stars, in tens) at ASM2115 for each sampling period (2–10 days, but usually 5 days) between May and December 2016. No samples are available for July and August. Both C_{max} and IF are positively related to D: $D = 0.00049 * C_{max} + 0.055 * IF$ ($R^2 = 0.69$, $p < 0.001$). (For interpretation of the references to colour in this figure legend, the reader is referred to the web version of this article.)

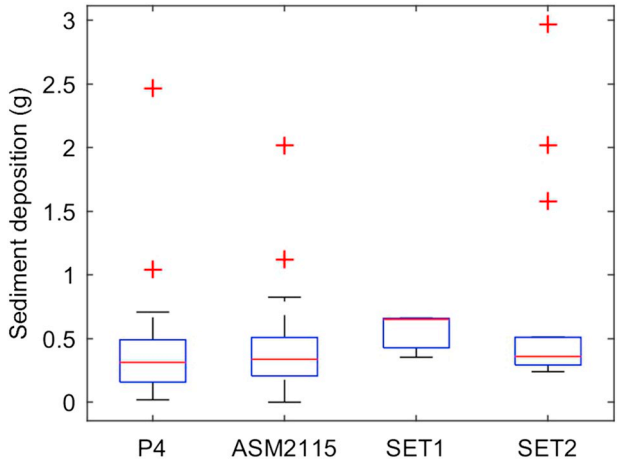

Fig. 6. Spatial pattern of average sediment deposition. Boxplot of sediment deposition (g) for all four filter-trap sites (P4, ASM2115, SET1 (during summer), SET2 (during autumn/winter), according to the map in Fig. 2), only accounting for periods, when inundation had occurred during at least one tide. Medians are represented by red lines, blue boxes indicate the 25th and 75th percentile (Q25 and Q75). Outliers (red crosses) are values larger than Q75 + 1.5 * (Q75–Q25). (For interpretation of the references to colour in this figure legend, the reader is referred to the web version of this article.)

sediment accretion rates were 17.4 ± 2.4 and 9.0 ± 2.8 mm yr^{-1} for the marker horizons (MH) at SET1 and SET2 respectively (Table 2: MH rates). These differences indicate that so-called 'shallow subsidence' (Cahoon et al., 1995), caused by sediment autocompaction (i.e. difference between MH and RSET rate), was much higher at site SET1 compared to site SET2. This enhanced compaction may be related to the closer vicinity of SET1 to the tidal creek network and the better drainage of the site, leading to higher invertebrate activity and greater void space below the SET1 surface. Additionally, the redox environments may be more favourable to decomposition of organics where oxygen availability is higher.

4.6. Long-term marsh edge dynamics

Margin retreat was found to be near-ubiquitous for the entire Dengie Peninsula with a mean rate of 1.93 m yr^{-1}. For the 60 m of marsh margin centred on the measurement transect, the 1992–2013 mean rate of retreat was 0.80 m yr^{-1} (standard deviation 0.23 m yr^{-1}). The region of maximum retreat (regularly exceeding 5.50 m yr^{-1}) was 1 km south of the study transect.

5. Discussion

5.1. Drivers of intertidal sediment resuspension

The supply of sediment as a vital control on the ability of coastal salt marshes to adapt to rising sea levels has widely been acknowledged in previous studies (Reed, 1989; French, 1993; French, 2006; Blum and Roberts, 2009; Weston, 2014). This study, conducted at a wave-exposed, macro-tidal coastal salt marsh on the UK east coast, shows that sediment availability of salt marshes is subject to pronounced temporal variability, with major variations in SSC on diurnal time scales. In contrast to systems dominated by tidal currents (e.g. Scheldt estuary: Fettweis et al., 1998; Severn estuary: Allen and Duffy, 1998), sediment supply on this marsh is primarily controlled by wave-induced sediment resuspension (Fig. 3), rather than resuspension caused by tidal currents, which were shown to be slower than the detection limit of our ADCP. Wave-induced sediment resuspension is triggered when the wave-induced bed shear stress exceeds the critical bed shear stress of the mudflat surface, a condition that is more likely to be met in shallow water conditions (Green and Coco, 2014).

In addition, the impact of wave activity on intertidal sediment resuspension varies seasonally, leading to higher SSCs in winter than in summer (Temmerman et al., 2003a, 2003b; Poirier et al., 2017). The weaker effect of wave activity on sediment resuspension during the summer months (Fig. 3) is likely related to the presence of seasonal biofilms (Underwood and Paterson, 1993; Paterson et al., 2000; Andersen, 2001; Tolhurst et al., 2008; Grabowski et al., 2011) and/or macroalgal mats (Frostick and McCave, 1979) covering the tidal mudflat, thereby reducing the erodibility of the mudflat surface.

Comparison of the seaward and landward turbidity during our experiment revealed a landward increase in SSC, indicating sediment resuspension in the near-salt marsh margin zone and subsequent landward sediment transport. This transport was significantly related to the depth-normalized wave activity, suggesting that waves initiate sediment resuspension and landward transport, particularly when water levels are low. Meanwhile, tidal currents appear not to play a significant role in onshore sediment transport, as they are of low magnitude compared to the prevailing wave activity. Similar wave-induced landward sediment transport has recently been reported for the Oosterschelde, NL (Ma et al., 2018). However at other sites, tidal currents have been shown to have a greater impact on landward sediment transport than wave activity (Janssen-Stelder, 2000; Zhu et al., 2014). Furthermore, some studies have emphasized the importance of longshore and cross-shore sediment advection for SSC and tidal mudflat topography (Wang et al., 2012; Shi et al., 2016). However, these advection terms have been shown to be most pronounced in the lower (seaward) parts of tidal mudflats (Le Hir et al., 2000; Wang et al.,

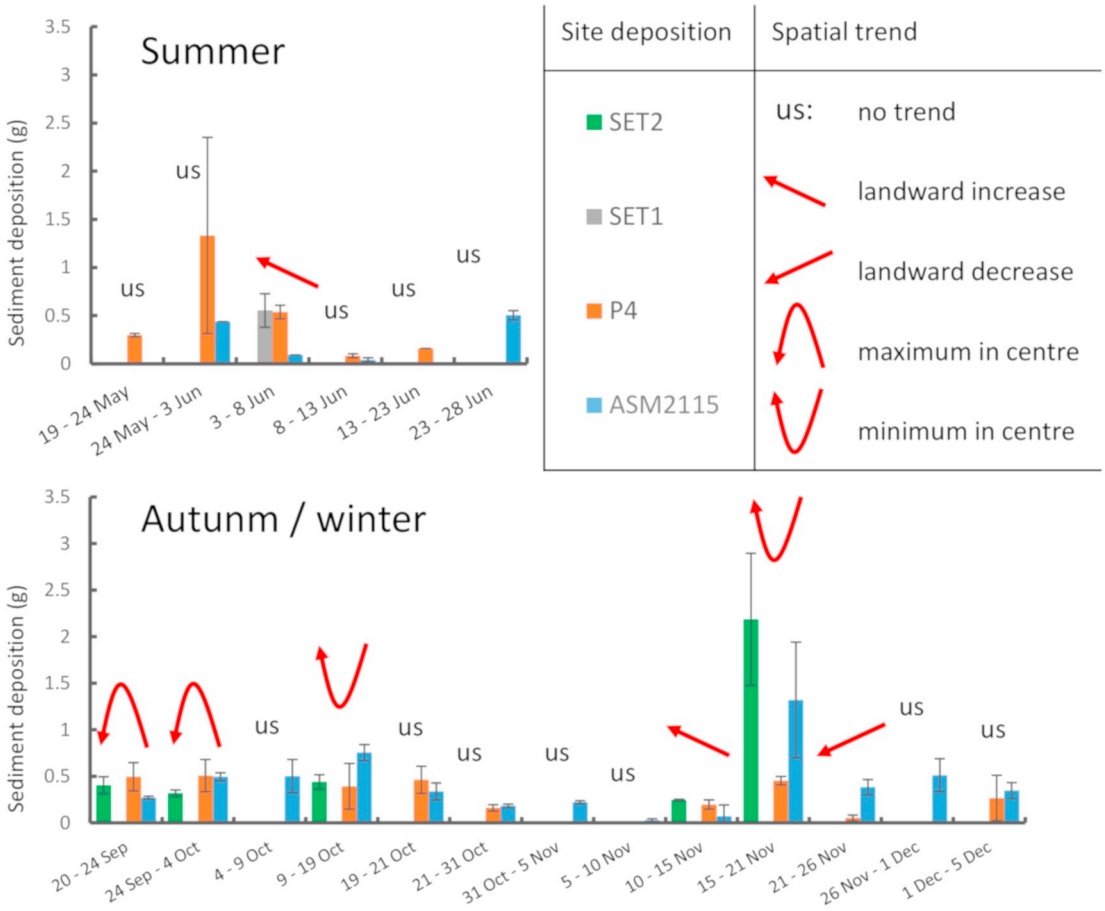

Fig. 7. Spatial patterns of individual sediment deposition events. Sediment deposition (g) from filter traps at four different locations on the salt marsh for every individual sampling period. Bars are shown in the order of the site's distances to the marsh edge: ASM2115 (blue bars): 0 m; P4 (orange bars): 23 m; SET1 (grey bars): 31 m; SET2 (green bars): 47 m. Error bars represent the standard deviation of up to three filters deployed per site. Significant spatial trends of sediment deposition are indicated by red arrows, insignificant trends by "us". (For interpretation of the references to colour in this figure legend, the reader is referred to the web version of this article.)

2012), with wind and current-induced sediment resuspension becoming more important towards the upper (landward) part of the tidal mudflat (Green, 2011; Ma et al., 2018). The latter position is where our measurements took place.

In previous studies, the erosion of tidal mudflats due to wave activity has widely been attributed to strong wind and storm events, with calm weather periods being responsible for intertidal sediment accretion, creating an equilibrium profile, adjusted to the prevailing wind and tide conditions (Janssen-Stelder, 2000; Le Hir et al., 2000). The data reported here, however, show little sign of elevation increases of the tidal mudflat during calm weather periods, and bed level changes are not significantly related to wave activity, a finding that is confirmed by recent data on mudflat elevation changes in various marsh system across the North Sea (Willemsen et al., 2018). The dominant signal is one of surface lowering, suggesting that the mudflat is out of equilibrium with prevailing energy conditions.

5.2. Sediment deposition on the marsh surface

The temporal variability of sediment deposition on the salt marsh surface was remarkably well correlated with the maximum SSC at the marsh edge and the inundation frequency of the marsh during each sampling period; when combined, these two variables explained 69% of the observed temporal variability in sediment deposition on the salt marsh. The maximum SSC for each sampling period thereby appears to be more important for surface deposition than the average SSC. Similar to previous studies on the vertical accretion of micro- and meso-tidal marshes (Bartholdy et al., 2004; Bellucci et al., 2007; Schuerch et al., 2013), this finding suggests that frequently occurring moderate to strong wind events, rather than extreme events or everyday tidal inundations, primarily control salt marsh sedimentation, at least in more seaward marsh locations. By contrast, in macro-tidal marshes, extreme storm-events have been shown to be more important for the vertical accretion of higher, interior marsh areas (French and Spencer, 1993; van Proosdij et al., 2006).

Given that the maximum SSC at the marsh edge is strongly related to the maximum increase in SSC between the turbidity sensors on the mudflat and at the marsh edge ($R^2 = 0.66$), the majority of the sediment delivered to the salt marsh must originate from the zone extending up to 130 m from the marsh edge, either from the tidal mudflat or the marsh edge (i.e. the shore-normal ridge and runnel system) itself. The narrowness of this zone is remarkable, given that the tidal mudflat adjacent to this part of the salt marsh extends seaward for 3.7 km. The exact relative contributions of sediment supplied from the erosion of the ridge and runnel system compared to sediment supplied from the erosion of the tidal mudflat cannot as yet be quantified. Our data, however, indicates a contribution from both source areas.

The removal of sediment from this area of the tidal mudflat during increased wave activity is also supported by the observed predominant lowering of the mudflat surface between the seaward and the landward turbidity sensors. However, unlike earlier suggestions (Le Hir et al., 2000), we show that much of this sediment is not removed from the system but transported landward onto the adjacent salt marsh where it is deposited. Also, the sediment seems not to originate from the marsh

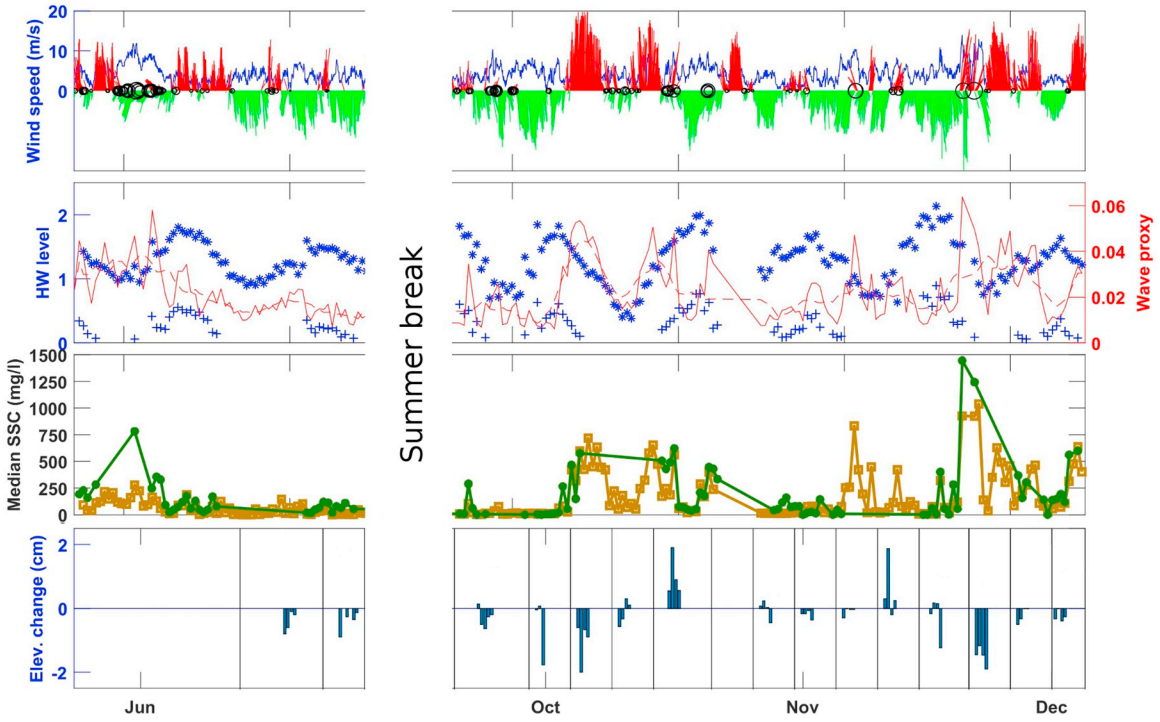

Fig. 8. Data time series. Time series of meteorological, hydrodynamic, SSC and mudflat morphology data for the entire measurement period. Top panel: prevailing wind conditions (blue: wind speed; red: onshore wind; green: offshore; black: cross-shore). 2nd panel: hydrodynamic forcing (stars: HW levels at ASM2113; crosses: HW levels at ASM2115; solid line: wave proxy at ASM2113; dashed line: smoothed wave proxy (moving average: 10 tides). 3rd panel: median SSC (brown squares: ASM2113; green circles: ASM2115). Bottom panel: mudflat morphodynamics (bars: net erosion (negative) and deposition (positive)). (For interpretation of the references to colour in this figure legend, the reader is referred to the web version of this article.)

edge only, as previously suggested (Reed, 1988); rather, the removal of the sediment actually lowers the mudflat surface.

The long-term measurements of sediment accretion and surface elevation change over the duration of the experiment confirm that sedimentation rates at the salt marsh are high compared to the long-term regional SLR rate of ca. 2.23 mm yr^{-1} (for Sheerness (Fig. 1) during the period 1901–2006, reported by Woodworth et al., 2009). The salt marsh therefore appears to represent a healthy tidal wetland with respect to its ability to vertically adapt to rising sea levels. However, the fact that the marsh's apparent ability to adapt to SLR is due to the removal of sediment from the marsh edge and the adjacent tidal mudflat in very close vicinity of the salt marsh edge, shows that the marsh is less resilient to SLR than anticipated from the vertical accretion rates alone (Fig. 9). As a consequence, the mudflat surface is gradually being eroded, interrupted by episodic import events which (partly) replenish the removed sediment with sediment from sources further offshore. This process is particularly observed during periods of high HW levels and low wave activity (Fig. 8).

Sediment deposition on the marsh platform did not show any significant trends in relation to the distance to the marsh edge. One might expect a decrease in sediment deposition rates with increasing distance from the marsh edge (Christiansen et al., 2000; Temmerman et al., 2003a, 2003b; van Proosdij et al., 2006; Poirier et al., 2017), but our data does not show any such trend. Instead, the sediment that is resuspended on the tidal mudflat is distributed into the salt marsh both via the marsh edge and through the complex channel network, leading to uniform sediment deposition within the most seaward 47 m of the marsh. The distribution of suspended sediment this far into the salt marsh is likely related to the wave exposure of the study site, as sediment that is initially deposited on the marsh surface may be resuspended and washed away during the same tide (Ma et al., 2018; Reef et al., 2018). With increasing inland distance, this effect becomes weaker as wave heights and energies are rapidly reduced when travelling over the vegetated marsh surface (Möller and Spencer, 2002).

5.3. Implication for long-term salt marsh morphological development

Previous studies have highlighted the importance of intertidal sediment resuspension as a driver for sediment availability of coastal salt marshes (Schuerch et al., 2013; Schuerch et al., 2014; Ma et al., 2018) and the possibility that vertical sediment accretion may occur through redistribution of sediment from the tidal mudflat and the marsh edge

Table 2
Long-term measurements of the increase in vertical salt marsh elevation (RSET reading) and sediment accretion (MH reading) at the sites SET1 and SET2, derived from the Rod Surface-Elevation Tables (RSET) and the Marker Horizons (MH), respectively.

Date	Site	RSET average (mm)[a]	RSET std.	SET (± 1 standard error) rate (mm yr^{-1})	MH average (mm)[a]	MH std.	MH (± 1 standard error) rate (mm yr^{-1})
18/12/2015	SET1	0.00	7.86	5.6 (± 1.5)	0.00	5.21	17.4 (± 2.4)
11/07/2016	SET1	6.89	7.33		6.83	7.91	
17/02/2017	SET1	6.64	6.90		20.25	7.44	
18/12/2015	SET2	0.00	13.51	5.3 (± 2.3)	0.00	7.39	9.0 (± 2.8)
11/07/2016	SET2	2.44	11.44		5.42	6.44	
17/02/2017	SET2	6.19	9.91		10.50	10.13	

[a] RSETs and MHs were installed in 2012 - readings reported here were reset to start at zero in December 2015.

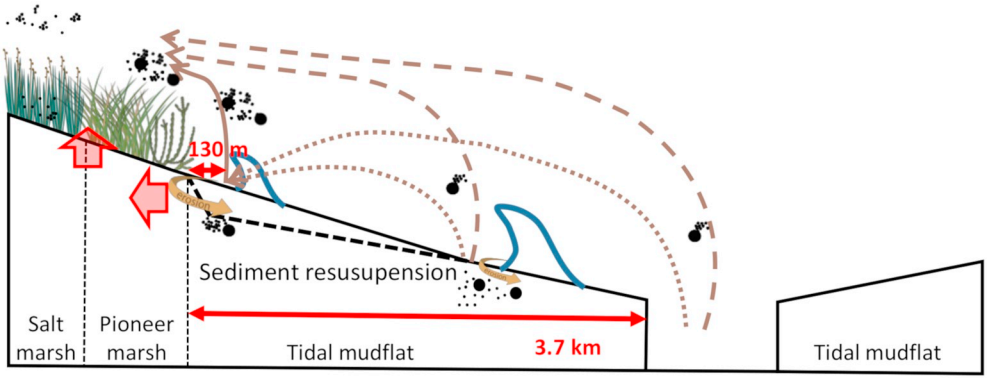

Fig. 9. Conceptual model. Schematic view of the implications of our data for the long-term morphological development of the salt marsh. The continuous arrow indicates the primary mechanism controlling the temporal variability of sediment supply to the salt marsh, dashed arrows indicate other possible mechanisms for sediment delivery (Schuerch et al., 2014), here found to be insignificant and the dotted arrows indicate the occasional replenishment of the near-edge tidal mudflat from either the lower tidal mudflat or external sources. The expected future topography is indicated by the dashed profile line.

(Mariotti and Carr, 2014). The fact that the deposited sediment is withdrawn from the marsh edge and the mudflat directly adjacent to the marsh edge, however, implies a much stronger negative effect of this sediment redistribution process on the overall morphological development of the salt marsh, if the removed sediment is not entirely replenished (Fig. 9). The coastal slope increases much faster than if the sediments were to originate from the wider tidal mudflat. Such an increased coastal slope inevitably increases the wave heights of incoming waves (Fagherazzi and Wiberg, 2009) and the susceptibility of the salt marsh to landward retreat (Callaghan et al., 2010; Mariotti and Fagherazzi, 2010; Fig. 9).

Based on modelling studies, periods of lateral salt marsh erosion have been suggested either as part of a cyclic behaviour of coastal salt marshes, where erosional phases are followed by vegetation re-establishment and seaward expansion of the marsh (van de Koppel et al., 2005), or as a transition from one stable state to another stable state, after a threshold condition has been exceeded (Mariotti and Fagherazzi, 2010). These thresholds are site dependent in magnitude, but usually depend on the rate of relative SLR, general sediment availability, nearshore bathymetry, sediment characteristics and prevailing wind climate (Mariotti and Carr, 2014).

In our study region (i.e. the Dengie Peninsula), a general trend of lateral marsh retreat (erosion) has been reported since 1953, following an extensive period of rapid expansion between 1870 and 1953 (van der Wal and Pye, 2004). The post-1953-period has been characterized by both periods of very rapid retreat (ca. 16 ha yr^{-1} from 1970 to 1973 and 20 ha yr^{-1} from 1953 to 1960), times of reduced loss rates (ca. 9 ha yr^{-1} from 1978 and 1981 and ca. 2.5 ha yr^{-1} since 1981), and occasionally even slow progradation (Greensmith and Tucker, 1965; Harmsworth and Long, 1986; Cooper et al., 2001; van der Wal and Pye, 2004). Currently, our data suggest maximum marsh edge retreat rates of up to 5.5 m yr^{-1} at the widest part of the marsh, falling to 0.8 m yr^{-1} on the transect of this experiment. Unlike the classical erosion of a marsh cliff (van de Koppel et al., 2005; Marani et al., 2011), the lateral erosion of this salt marsh is characterized by the erosion of the ridge-runnel system (Greensmith and Tucker, 1966) as well as the seaward tidal mudflat. The formation and erosion of the ridge-runnel system has been suggested to be part of the cyclic behaviour of marsh edge retreat and progradation, assuming that the sediment removed from the marsh edge during lateral erosion, is deposited on the tidal mudflat in front of the marsh edge, enabling the marsh to re-establish once the mudflat elevation is sufficiently high (Greensmith and Tucker, 1966).

Our data, however, show that the majority of the sediment removed from the marsh edge and the mudflat is deposited on the marsh surface, not on the tidal mudflat, suggesting that rather than being a temporary erosional phase, the mudflat-salt marsh system in Tillingham is out of equilibrium with the current physical setting. Based on the available data, we can therefore not conclusively establish whether this instability is part of a cyclic behaviour on decadal timescales or if it indicates the system's adaptation to a new equilibrium with a reduced salt marsh area, in response to an environmental threshold being exceeded. Possible reasons for threshold exceedance are either a reduction in the general sediment availability of the broader coastal environment (e.g. reduction in riverine sediment discharge), a long-term change in longshore sediment transport (e.g. due to changes in the wind/wave climate), geomorphological changes within the broader coastal shelf environment (e.g. shifting subtidal sand ridges and channels in the Greater Thames estuary), or the local SLR rate exceeding the ability of this system to adapt to changes in external forcing.

The continuous loss of salt marsh area through lateral erosion despite the high sedimentation rates observed on the marsh surface highlights the close coupling of the sediment dynamics on the tidal mudflat with those on the marsh surface. Salt marsh sedimentation and elevation growth rates alone, often used to assess the ability of salt marshes to adapt to future SLR (Webb et al., 2013), are therefore an unsuitable tool for assessing the response of a salt marsh to SLR. When considering the ability of coastal salt marshes to adapt to global SLR, it is therefore crucially important to not only consider the morphological development of the salt marsh, but the salt marsh should also be considered as part of a coupled tidal mudflat-salt marsh system.

6. Conclusions

On the Dengie Peninsula (UK), sediment availability for the vertical accretion of the marsh has been shown to be highly variable in time and primarily controlled by wave activity. The recorded suspended sediment concentrations are particularly high during moderate to high wave events in the winter months, therefore enabling the marsh to vertically grow at a pace that exceeds the long-term, regional rate of SLR. The contributed sediment, however, has been shown to originate from the marsh edge and the tidal mudflat directly adjacent to the salt marsh, namely within 130 m from the marsh edge (whereas the entire mudflat is 3.7 km wide), causing a lowering of the mudflat surface. The simultaneous increase in marsh elevation and the erosion of the mudflat surface causes an increase in coastal slope and facilitates lateral marsh edge erosion, a process that has long been observed on this marsh. Our results show that vertical sediment accretion and surface elevation change alone are no indicators of resilience to SLR for coastal salt marshes. Rather, it is necessary to assess the morphological development of the entire tidal mudflat-salt marsh system to understand how resilient a coastal salt marsh really is to environmental forcing.

Acknowledgments

We thank Athanasios Vafeidis and Roberto Mayerle from the Christian-Albrechts-University of Kiel (“The Future Ocean” Excellence Cluster) for access to field equipment. At the Department of Geography, Cambridge University we thank Chris Rolfe, Steve Boreham and Adam Copeland for support in conducting field and laboratory data collection; Elizabeth Christie, James Tempest and Ruth Reef for help during data

collection in the field; and Iris Möller for her valuable comments.

Funding

This work was supported by the German Research Foundation - DFG [grant no: 272052902] and by the Cambridge Coastal Research Unit (Visiting Scholar Programme to MS). Additional support was received from the European Commission under the FP7 project Foreshore Assessment Using Space Technology [grant no: 607131] as well as the NERC-funded projects Coastal Biodiversity and Ecosystem Services Sustainability (CBESS; grant no: NE/J015423/1) and BLUE-coast (grant no: NE/N015878/1).

Data availability

Datasets related to this article can be found at *[Link to Mendeley Data]*, an open-source online data repository hosted at Mendeley Data.

References

Allen, J.R.L., 2000. Morphodynamics of Holocene salt marshes: a review sketch from the Atlantic and Southern North Sea coasts of Europe. Quat. Sci. Rev. 19, 1155–1231.
Allen, J.R.L., Duffy, M.J., 1998. Medium-term sedimentation on high intertidal mudflats and salt marshes in the Severn Estuary, SW Britain: the role of wind and tide. Mar. Geol. 150, 1–27.
Andersen, T.J., 2001. Seasonal variation in erodibility of Two temperate, microtidal Mudflats. Estuar. Coast. Shelf Sci. 53, 1–12.
Barbier, E.B., Hacker, S.D., Kennedy, C., Koch, E.W., Stier, A.C., Silliman, B.R., 2011. The value of estuarine and coastal ecosystem services. Ecol. Monogr. 81, 169–193.
Bartholdy, J., Christiansen, C., Kunzendorf, H., 2004. Long term variations in backbarrier salt marsh deposition on the Skallingen peninsula – the Danish Wadden Sea. Mar. Geol. 203, 1–21.
Bellucci, L.G., Frignani, M., Cochran, J.K., Albertazzi, S., Zaggia, L., Cecconi, G., Hopkins, H., 2007. ^{210}Pb and ^{137}Cs as chronometers for salt marsh accretion in the Venice Lagoon – links to flooding frequency and climate change. J. Environ. Radioact. 97, 85–102.
Bergamino, L., Schuerch, M., Tudurí, A., Carretero, S., García-Rodríguez, F., 2017. Linking patterns of freshwater discharge and sources of organic matter within the Río de la Plata estuary and adjacent marshes. Mar. Freshw. Res. 68, 1704–1715.
Blum, M.D., Roberts, H.H., 2009. Drowning of the Mississippi Delta due to insufficient sediment supply and global sea-level rise. Nat. Geosci. 2, 488–491.
Cahoon, D.R., Reed, D.J., Day, J.W., 1995. Estimating shallow subsidence in microtidal salt marshes of the southeastern United States: Kaye and Barghoorn revisited. Mar. Geol. 128, 1–9.
Cahoon, D.R., Lynch, J.C., Perez, B.C., Segura, B., Holland, R.D., Stelly, C., Stephenson, C., Hensel, P., 2002. High-precision measurements of wetland sediment elevation: II. The rod surface elevation table. J. Sediment. Res. 72, 734–739.
Callaghan, D.P., Bouma, T.J., Klaassen, P., van der Wal, D., Stive, M.J.F., Herman, P.M.J., 2010. Hydrodynamic forcing on salt-marsh development: Distinguishing the relative importance of waves and tidal flows. Estuar. Coast. Shelf Sci. 89, 73–88.
Christiansen, T., Wiberg, P.L., Milligan, T.G., 2000. Flow and sediment transport on a tidal salt marsh surface. Estuar. Coast. Shelf Sci. 50, 315–331.
Church, J.A., Clark, P.U., Cazenave, A., Gregory, J.M., Jevrejeva, S., Levermann, A., Merrifield, M.A., Milne, G.A., Nerem, R.S., Nunn, P.D., Payne, A.J., Pfeffer, W.T., Stammer, D., Unnikrishnan, A.S., 2013. Sea Level Change. In: Stocker, T.F., Qin, D., Plattner, G.-K., Tignor, M., Allen, S.K., Boschung, J., Nauels, A., Xia, Y., Bex, V., Midgley, P.M. (Eds.), Climate Change 2013: The Physical Science Basis. Contribution of Working Group I to the Fifth Assessment Report of the Intergovernmental Panel on Climate Change. Cambridge University Press, Cambridge, United Kingdom and New York, NY, USA.
Cooper, N.J., Cooper, T., Burd, F., 2001. 25 years of salt marsh erosion in Essex: Implications for coastal defence and nature conservation. J. Coast. Conserv. 7, 31–40.
Crosby, S.C., Sax, D.F., Palmer, M.E., Booth, H.S., Deegan, L.A., Bertness, M.D., Leslie, H.M., 2016. Salt marsh persistence is threatened by predicted sea-level rise. Estuar. Coast. Shelf Sci. 181, 93–99.
D'Alpaos, A., Lanzoni, S., Marani, M., Rinaldo, A., 2007. Landscape evolution in tidal embayments: modeling the interplay of erosion, sedimentation, and vegetation dynamics. J. Geophys. Res. Earth Surf. 112, F01008.
D'Alpaos, A., Mudd, S.M., Carniello, L., 2011. Dynamic response of marshes to perturbations in suspended sediment concentrations and rates of relative sea level rise. J. Geophys. Res. Earth Surf. 116, F04020.
van de Koppel, J., van der Wal, D., Bakker, J.P., Herman, P.M.J., 2005. Self-organization and vegetation collapse in salt marsh ecosystems. Am. Nat. 165, E1–E12.
van der Wal, D., Pye, K., 2004. Patterns, rates and possible causes of saltmarsh erosion in the Greater Thames area (UK). Geomorphology 61, 373–391.
Environment Agency, 2016a. Vertical Aerial Photography Tiles - RGBN. Environment Agency.
Environment Agency, 2016b. LIDAR Tiles Digital Terrain Model (DTM). Environment Agency.
Fagherazzi, S., Wiberg, P.L., 2009. Importance of wind conditions, fetch, and water levels on wave-generated shear stresses in shallow intertidal basins. J. Geophys. Res. Earth Surf. 114, F03022.
Fettweis, M., Sas, M., Monbaliu, J., 1998. Seasonal, Neap-spring and Tidal Variation of Cohesive Sediment Concentration in the Scheldt Estuary, Belgium. Estuar. Coast. Shelf Sci. 47, 21–36.
French, J.R., 1993. Numerical simulation of vertical marsh growth and adjustment to accelerated sea-level rise, North Norfolk, U.K. Earth Surf. Process. Landf. 18, 63–81.
French, J., 2006. Tidal marsh sedimentation and resilience to environmental change: Exploratory modelling of tidal, sea-level and sediment supply forcing in predominantly allochthonous systems. Mar. Geol. 235, 119–136.
French, J.R., Spencer, T., 1993. Dynamics of sedimentation in a tide-dominated back-barrier salt marsh, Norfolk, UK. Mar. Geol. 110, 315–331.
Friedrichs, C.T., Perry, J.E., 2001. Tidal salt marsh morphodynamics: a synthesis. J. Coast. Res. 7–37.
Frostick, L.E., McCave, I.N., 1979. Seasonal shifts of sediment within an estuary mediated by algal growth. Estuar. Coast. Mar. Sci. 9, 569–576.
Grabowski, R.C., Droppo, I.G., Wharton, G., 2011. Erodibility of cohesive sediment: the importance of sediment properties. Earth Sci. Rev. 105, 101–120.
Green, M.O., 2011. Very small waves and associated sediment resuspension on an estuarine intertidal flat. Estuar. Coast. Shelf Sci. 93, 449–459.
Green, M.O., Coco, G., 2014. Review of wave-driven sediment resuspension and transport in estuaries. Rev. Geophys. 52, 77–117.
Greensmith, J.T., Tucker, E.V., 1965. Salt marsh erosion in Essex. Nature 206, 606.
Greensmith, J.T., Tucker, E.V., 1966. Morphology and evolution of inshore shell ridges and mud-mounds on modern intertidal flats, near Bradwell, Essex. Proc. Geol. Assoc. 77, 329–IN326.
Harmsworth, G.C., Long, S.P., 1986. An assessment of saltmarsh erosion in Essex, England, with reference to the Dengie Peninsula. Biol. Conserv. 35, 377–387.
Hill, T.D., Anisfeld, S.C., 2015. Coastal wetland response to sea level rise in Connecticut and New York. Estuar. Coast. Shelf Sci. 163, 185–193.
Janssen-Stelder, B., 2000. The effect of different hydrodynamic conditions on the morphodynamics of a tidal mudflat in the Dutch Wadden Sea. Cont. Shelf Res. 20, 1461–1478.
Kirwan, M.L., Guntenspergen, G.R.C.F., 2010. Influence of tidal range on the stability of coastal marshland. J. Geophys. Res. Earth Surf. 115, F02009.
Kirwan, M.L., Murray, A.B., 2007. A coupled geomorphic and ecological model of tidal marsh evolution. Proc. Natl. Acad. Sci. 104, 6118–6122.
Kirwan, M.L., Guntenspergen, G.R., D'Alpaos, A., Morris, J.T., Mudd, S.M., Temmerman, S., 2010. Limits on the adaptability of coastal marshes to rising sea level. Geophys. Res. Lett. 37, L23401.
Kolker, A.S., Kirwan, M.L., Goodbred, S.L., Cochran, J.K., 2010. Global climate changes recorded in coastal wetland sediments: Empirical observations linked to theoretical predictions. Geophys. Res. Lett. 37, L14706.
Le Hir, P., Roberts, W., Cazaillet, O., Christie, M., Bassoullet, P., Bacher, C., 2000. Characterization of intertidal flat hydrodynamics. Cont. Shelf Res. 20, 1433–1459.
Ma, Z., Ysebaert, T., Wal, D., Herman, P.M.J., 2018. Conditional Effects of Tides and Waves on Short-term Marsh Sedimentation Dynamics. Earth Surface Processes and Landforms, Early View.
Marani, M., D'Alpaos, A., Lanzoni, S., Santalucia, M., 2011. Understanding and predicting wave erosion of marsh edges. Geophys. Res. Lett. 38.
Mariotti, G., Carr, J., 2014. Dual role of salt marsh retreat: Long-term loss and short-term resilience. Water Resour. Res. 50, 2963–2974.
Mariotti, G., Fagherazzi, S., 2010. A numerical model for the coupled long-term evolution of salt marshes and tidal flats. J. Geophys. Res. Earth Surf. 115, F01004.
Met Office, 2006. MIDAS: UK Hourly Weather Observation Data. NCAS British Atmospheric Data Centre.
Möller, I., 2006. Quantifying saltmarsh vegetation and its effect on wave height dissipation: results from a UK East coast saltmarsh. Estuar. Coast. Shelf Sci. 69, 337–351.
Möller, I., Spencer, T., 2002. Wave dissipation over macro-tidal saltmarshes: effects of marsh edge typology and vegetation change. J. Coast. Res. 36, 506–521.
Möller, I., Spencer, T., French, J.R., Leggett, D.J., Dixon, M., 1999. Wave transformation over salt marshes: a field and numerical modelling study from North Norfolk, England. Estuar. Coast. Shelf Sci. 49, 411–426.
Nolte, S., Koppenaal, E.C., Esselink, P., Dijkema, K.S., Schuerch, M., De Groot, A.V., Bakker, J.P., Temmerman, S., 2013. Measuring sedimentation in tidal marshes: a review on methods and their applicability in biogeomorphological studies. J. Coast. Conserv. 17, 301–325.
Paterson, D.M., Tolhurst, T.J., Kelly, J.A., Honeywill, C., de Deckere, E.M.G.T., Huet, V., Shayler, S.A., Black, K.S., de Brouwer, J., Davidson, I., 2000. Variations in sediment properties, Skeffling mudflat, Humber Estuary, UK. Cont. Shelf Res. 20, 1373–1396.
Pedersen, J.B.T., Bartholdy, J., 2006. Budgets for fine-grained sediment in the Danish Wadden Sea. Mar. Geol. 235, 101–117.
Poirier, E., van Proosdij, D., Milligan, T.G., 2017. The effect of source suspended sediment concentration on the sediment dynamics of a macrotidal creek and salt marsh. Cont. Shelf Res. 148, 130–138.
van Proosdij, D., Davidson-Arnott, R.G.D., Ollerhead, J., 2006. Controls on spatial patterns of sediment deposition across a macro-tidal salt marsh surface over single tidal cycles. Estuar. Coast. Shelf Sci. 69, 64–86.
Reed, D.J., 1988. Sediment dynamics and deposition in a retreating coastal salt marsh. Estuar. Coast. Shelf Sci. 26, 67–79.
Reed, D.J., 1989. Patterns of sediment deposition in subsiding coastal salt marshes, Terrebonne Bay, Louisiana: the role of winter storms. Estuaries 12, 222–227.
Reef, R., Schuerch, M., Christie, E.K., Möller, I., Spencer, T., 2018. The effect of vegetation height and biomass on the sediment budget of a European saltmarsh. Estuar. Coast. Shelf Sci. 202, 125–133.
Rodríguez, J.F., Saco, P.M., Sandi, S., Saintilan, N., Riccardi, G., 2017. Potential increase

in coastal wetland vulnerability to sea-level rise suggested by considering hydrodynamic attenuation effects. Nat. Commun. 8, 16094.
Runte, K., 1989. Methodische verfahren zur quantifizierung von umlagerungen in intertidalen sedimenten. Meyniana 41, 153–165.
Schepers, L., Kirwan, M., Guntenspergen, G., Temmerman, S., 2017. Spatio-temporal development of vegetation die-off in a submerging coastal marsh. Limnol. Oceanogr. 62, 137–150.
Schuerch, M., Vafeidis, A., Slawig, T., Temmerman, S., 2013. Modeling the influence of changing storm patterns on the ability of a salt marsh to keep pace with sea level rise. J. Geophys. Res. Earth Surf. 118, 84–96.
Schuerch, M., Dolch, T., Reise, K., Vafeidis, A.T., 2014. Unravelling interactions between salt marsh evolution and sedimentary processes in the Wadden Sea (southeastern North Sea). Prog. Phys. Geogr. 38, 691–715.
Schuerch, M., Scholten, J., Carretero, S., García-Rodríguez, F., Kumbier, K., Baechtiger, M., Liebetrau, V., 2016. The effect of long-term and decadal climate and hydrology variations on estuarine marsh dynamics: an identifying case study from the Río de la Plata. Geomorphology 269, 122–132.
Schuerch, M., Spencer, T., Temmerman, S., Kirwan, M.L., Wolff, C., Lincke, D., McOwen, C.J., Pickering, M.D., Reef, R., Vafeidis, A.T., Hinkel, J., Nicholls, R.J., Brown, S., 2018. Future response of global coastal wetlands to sea level rise. Nature 561, 231–234.
Schwarzer, K., Diesing, M., Larson, M., Niedermeyer, R.O., Schumacher, W., Furmanczyk, K., 2003. Coastline evolution at different time scales – examples from the Pomeranian Bight, southern Baltic Sea. Mar. Geol. 194, 79–101.
Shi, B., Wang, Y.P., Du, X., Cooper, J.R., Li, P., Li, M.L., Yang, Y., 2016. Field and theoretical investigation of sediment mass fluxes on an accretional coastal mudflat. J. Hydro Environ. Res. 11, 75–90.
Spencer, T., Schuerch, M., Nicholls, R.J., Hinkel, J., Lincke, D., Vafeidis, A.T., Reef, R., McFadden, L., Brown, S., 2016. Global coastal wetland change under sea-level rise and related stresses: the DIVA Wetland Change Model. Glob. Planet. Chang. 139, 15–30.
Stevenson, J.C., Ward, L.G., Kearney, M.S., 1986. Vertical accretion in marshes with varying rates of sea level rise. In: Wolfe, D.A. (Ed.), Estuarine Variability. Academic Press Inc., Orlando, Florida, pp. 241–259.
Temmerman, S., Govers, G., Meire, P., Wartel, S., 2003a. Modelling long-term tidal marsh growth under changing tidal conditions and suspended sediment concentrations, Scheldt estuary, Belgium. Mar. Geol. 193, 151–169.
Temmerman, S., Govers, G., Wartel, S., Meire, P., 2003b. Spatial and temporal factors controlling short-term sedimentation in a salt and freshwater tidal marsh, Scheldt estuary, Belgium, SW Netherlands. Earth Surf. Process. Landf. 28, 739–755.
Thieler, E.R., Himmelstoss, E.A., Zichichi, J.L., Ergul, A., 2009. The Digital Shoreline Analysis System (DSAS) Version 4.0 - An ArcGIS Extension for Calculating Shoreline Change. (Open-File Report, - ed, Reston).
Tolhurst, T.J., Consalvey, M., Paterson, D.M., 2008. Changes in cohesive sediment properties associated with the growth of a diatom biofilm. Hydrobiologia 596, 225–239.
Towler, P., Fishwick, M., 2017. Reeds Nautical Almanac 2018. Bloomsbury Publishing Plc, London.
Underwood, G.J.C., Paterson, D.M., 1993. Seasonal changes in diatom biomass, sediment stability and biogenic stabilization in the Severn Estuary. J. Mar. Biol. Assoc. U. K. 73, 871–887.
Wang, Y.P., Gao, S., Jia, J., Thompson, C.E.L., Gao, J., Yang, Y., 2012. Sediment transport over an accretional intertidal flat with influences of reclamation, Jiangsu coast, China. Mar. Geol. 291-294, 147–161.
Webb, E.L., Friess, D.A., Krauss, K.W., Cahoon, D.R., Guntenspergen, G.R., Phelps, J., 2013. A global standard for monitoring coastal wetland vulnerability to accelerated sea-level rise. Nat. Clim. Chang. 3, 458–465.
Weston, N.B., 2014. Declining sediments and rising seas: an unfortunate convergence for tidal wetlands. Estuar. Coasts 37, 1–23.
Willemsen, P.W.J.M., Borsje, B.W., Hulscher, S.J.M.H., van der Wal, D., Zhu, Z., Oteman, B., Evans, B., Möller, I., Bouma, T.J., 2018. Quantifying bed level change at the transition of tidal flat and salt marsh: can we understand the lateral location of the Marsh Edge? J. Geophys. Res. Earth Surf. 123. https://doi.org/10.1029/2018JF004742.
Woodworth, P.L., Teferle, F.N., Bingley, R.M., Shennan, I., Williams, S.D.P., 2009. Trends in UK mean sea level revisited. Geophys. J. Int. 176, 19–30.
Zhou, Z., Ye, Q., Coco, G., 2016. A one-dimensional biomorphodynamic model of tidal flats: Sediment sorting, marsh distribution, and carbon accumulation under sea level rise. Adv. Water Resour. 93, 288–302.
Zhu, Q., Yang, S., Ma, Y., 2014. Intra-tidal sedimentary processes associated with combined wave–current action on an exposed, erosional mudflat, southeastern Yangtze River Delta, China. Mar. Geol. 347, 95–106.